Computational Materials Science 117 (2016) 338–353

Contents lists available at ScienceDirect

Computational Materials Science

journal homepage: www.elsevier.com/locate/commatsci

A molecular characterization of hyper-cross-linked hybrid polyPOSS-imide networks

Sylvie Neyertz [a,b,*], David Brown [a,b], Michiel J.T. Raaijmakers [c], Nieck E. Benes [c]

[a] LEPMI, University Savoie Mont Blanc, F-73000 Chambéry, France
[b] LEPMI, CNRS, F-38000 Grenoble, France
[c] Inorganic Membranes, Department of Science and Technology, MESA+ Institute for Nanotechnology, University of Twente, P.O. Box 217, 7500 AE Enschede, The Netherlands

ARTICLE INFO

Article history:
Received 4 January 2016
Accepted 10 February 2016

Keywords:
Molecular dynamics (MD) simulations
Cross-linking
POSS
Imide
Polycondensation
Imidization

ABSTRACT

Hybrid hyper-cross-linked membranes based on inorganic polyhedral oligomeric silsesquioxanes (POSS) covalently bonded with organic imides have been shown to maintain remarkable molecular sieving abilities and gas separation performances up to 300 °C. These films are obtained through the interfacial polycondensation of POSS with a dianhydride, leading to a polyPOSS-(amic acid) network, which is then converted to a polyPOSS-imide network by thermal imidization. Using the pyromellitic (PMDA) dianhydride as a test case, the underlying molecular structures have been generated by molecular dynamics (MD) simulations and specific algorithms which closely mimicked the mixing, polycondensation and imidization steps of the experimental scheme. This allowed realistic models of the final cross-linked imide networks to be compared with their un-cross-linked monomer mixtures and their intermediate amic-acid precursors. Both the formation of the network and the subsequent imidization decreased the density as the systems became sterically more constrained. The volume shrinkage during imidization was less than expected considering the amount of water removal. This led to a larger void space and an improved gas solubility for the polyPOSS-imide films. Although the networks were constructed with the experimentally-found average of four linked arms per POSS, the distribution of the number of links per POSS were quite wide with a range from zero to the maximum possible of eight links per POSS. There was also considerable heterogeneity in the POSS···imide···POSS angles, which was related to the flexible aliphatic linker between the organic and inorganic moieties. Thermomechanical analyses confirmed that these cross-linked materials were well-suited for high-temperature applications. When subjected to uniaxial tension, they strain hardened at large deformations and their elastic moduli remained solid-like at high temperatures.

1. Introduction

Gas separation by nonporous glassy polymeric membranes has long been investigated as an alternative to the more conventional cryogenic distillation or adsorption separation processes because of the smaller sizes of the membrane devices and their lower energy costs. Their main applications include the separation of common gases such as O_2, N_2, He, H_2, CH_4 or CO_2 from air, natural gas, flue gas, syngas or other petrochemical products [1,2]. Many gas permeabilities and selectivities of polymer membranes have been reported in the literature [2,3], but most of them were measured at 25–35 °C. On the other hand, some industrial applications such as the treatment of syngas directly from the water gas shift reactor or the treatment of power plant flue gas involve processes at much higher temperatures [4].

There are only very few polymers, among which polyimides [5] and their thermally-rearranged derivatives [6,7], which are able to maintain gas molecular sieving abilities at temperatures of 200–300 °C. High-performance polymers can also be crosslinked, which suppresses plasticization and improves resistance [8]. However, inorganic materials usually exhibit even better thermomechanical properties. As such, hybrid materials based on both organic and inorganic moieties have gained attention for potentially combining good gas separation properties along with thermomechanical resistances and cost-efficiencies [9]. These so-called hybrid organic–inorganic membranes include both the blends in which the inorganic phases are physically dispersed in the organic matrices [10], as well as the networks in which the inorganic and

* Corresponding author at: LEPMI, University Savoie Mont Blanc, F-73000 Chambéry, France.
E-mail address: sylvie.neyertz@univ-smb.fr (S. Neyertz).

http://dx.doi.org/10.1016/j.commatsci.2016.02.015
0927-0256/

organic components are linked through strong ionic or covalent bonding [11].

Polyhedral oligomeric silsesquioxanes (POSS) [12], with the basic formula $(RSiO_{3/2})_n$ are one of the emerging classes of hybrid organic–inorganic materials for controlled gas transport properties [13]. They are based on rigid inorganic siloxane cages functionalized with flexible organic substituents R at their corners. There are many different POSS depending on the nature of R and the value of n, which typically varies from 6 to 16 [14]. However, the most extensively studied up to date are the cubic POSS with $n = 8$, i.e. Si_8O_{12} cages functionalized with eight pendant organic arms [12]. Within the context of permeation, small gas molecules can move through the intertwined organic chains [13], but POSS are rarely studied on their own since their membrane-forming capacities are limited. On the other hand, gas transport properties have been investigated for polymeric membranes that use either POSS as physical fillers or covalently bonded with organic moieties of various lengths [9,15–18]. In both types of materials, these hybrid membranes can include oligo- or polyimides as the organic component [19–22]. Poly(imide silsesquioxane)s also find applications in other high-performance domains [23], such as fuel cells [24,25] or space survivability [26].

Recently, Raaijmakers, Benes and coworkers have developed a method for the facile production of ultrathin and hyper-cross-linked films consisting of networks of POSS covalently bound with organic imide moities [27–30]. This approach is based [31] on the polycondensation of a primary amine-functionalized POSS with a dianhydride at the interface between two immiscible solvents, which results in the formation of an homogeneous polyPOSS-(amic acid) film. The amic acid groups are then converted into cyclic imide groups via thermal imidization at temperatures up to 300 °C, thus producing a defect-free polyPOSS-imide thin film. This method has been applied to various dianhydride linkers and shown to lead to hyper-cross-linked networks with tailored molecular sieving capabilities, which are able to maintain gas separation performances up to 300 °C. In addition, the facile synthesis conditions and the defect-free processability are well adapted to large-scale production [27–30].

The high thermal stabilities of those polyPOSS-imides have been attributed to the hyper-cross-linked nature of the thin films. It has been shown using X-ray photoelectron spectroscopy (XPS) that on average, four out of the eight functional groups on each POSS react with a dianhydride, the four remaining groups mainly consist of amines, and both anhydride groups on each dianhydride are converted to cyclic imide bonds [27,28,30]. However, it is unclear how the actual linkages are distributed within the material at the molecular level. The present work thus attempts to bridge the gap between the experimental characterizations and the underlying molecular structures by using molecular dynamics (MD) simulations and construction algorithms which closely mimick the entire experimental reaction scheme. The pyromellitic (PMDA) dianhydride is chosen here as a test case. Molecular models of amino-functionalized POSS and PMDA dianhydrides are first prepared separately at room temperature and then put into contact to represent the initial conditions for interfacial polycondensation. Several algorithms are tested to carry out the actual polycondensation reaction and create the intermediate polyPOSS-(amic acid) networks. The models are then heated up and subjected to an algorithm which converts the amic groups into cyclic imide groups, thus creating the final model polyPOSS-imides films.

Molecular models of cross-linked materials are usually based on heuristic distance criteria with various relaxation procedures [32]. Essentially two approaches have been used to create networks from atomistic models of the mixtures of the reacting molecules, most of them related to epoxy-based thermosets [33–44]: (i) formation of the entire network from a single static configuration and (ii) progressive formation of the network via alternating reaction and relaxation cycles. In the first case, the problem is essentially equivalent to solving the travelling salesman problem for which solutions exist, e.g. the simulated annealing technique [36,38]. The static approach inevitably leads to longer and longer initial bonds being defined as the degree of cross-linking is increased and considerable strain can end up being trapped in the resulting structures [33]. Progressive formation of the network can in part alleviate this problem as strains induced by creating long bonds are relaxed out. For example, it is possible to link a pair of sites at each reaction step before carrying out cycles of energy minimization and MD to shrink the newly created long bond and re-equilibrate the system [34]. Such a one-by-one approach is not entirely satisfactory in that the time required depends on the system size. Heine et al. [45] proposed a dynamic cross-linking method for poly(dimethylsiloxane) networks, where all reacting sites within a pre-specified range at each time step reacted in the course of an MD simulation with specific bonding potentials for the newly created bonds preventing instabilities developing in the dynamics. Varshney et al. [35] coupled the dynamic cross-linking concept with the iterative cycles of energy minimization and MD, along with a multistep relaxation procedure based on variable bonding force constants and distance criteria. Although there were differences in the details (for example the chosen cutoff for cross-linking), similar bond-forming/relaxation approaches have been applied successfully both to epoxies [36–38,41] and to other networks [46–48]. Several aspects have been further explored, such as the evolution of the partial atomic charges during curing [39], the formation of bonds being based on reaction kinetics instead of a distance criterion [40], or the use of a modified Lennard–Jones instead of a bond potential [42].

Coarse-graining approaches have also been used to create networks [36], most of the reported work dealing once again with epoxies [49–51]. These typically involve mapping the reaction mixture to a coarse-grained (CG) system, performing the network-forming reactions in the CG system and back-mapping to an atomistic model [49]. However, the mapping/reverse mapping procedures are far from being straightforward [52] and such elaborate approaches are mostly pertinent if the reaction rates become too slow in the atomistic system or if the diffusion of the reactants is important, e.g. through the formation of density gradients [50,51]. This is not necessary here as the POSS + PMDA mixtures are already solid-like and their reaction rates are known to be relatively fast: the resulting membranes are thin [27,29,30], i.e. the formation of the network is rapid with respect to the diffusion of the reacting species through the forming membrane. Finally, rather than starting from a monomer mixture, it also possible in both fully-atomistic and coarse-grained approaches to construct polymer chains in a first step and cross-link them in a second step, either directly or by adding linkers. This has been done for networks based on e.g. polyamide [32], polystyrene [53], polydimethylsiloxane [54] or liquid crystalline elastomers [55].

In the present case, we use a similar generic approach as the fully-atomistic bond-forming/relaxation procedure and apply it to the specific hyper-cross-linked POSS-imides under study. While some of the aforementioned simulations do include POSS moieties (usually at fairly low loadings) [36,38,47,48,54], the linkages based on single dianhydride moieties are hereby much shorter, thus leading to closer POSS···POSS distances. In addition, the novelty is that the cross-linking intermediate, the polyPOSS-(amic acid) form, is specifically simulated before being transformed into the final polyPOSS-imide form. The model networks are thus created in a way as close as possible to the experimental films and some input parameters, such as the stoechiometry and the degree of cross-linking, are provided by the experimental conditions.

The objective is to generate molecular models that are as realistic as possible with respect to the real hydrid poly(POSS-imide) films obtained by interfacial polymerization and thermal imidization. Structural and thermomechanical analyses are used to compare the final cross-linked imide networks with their un-cross-linked monomer mixtures and their cross-linked amic-acid precursors.

2. The experimental process reaction scheme

The formation of polyPOSS-(amic acid) and polyPOSS-imide macromolecular networks has been extensively described in Refs. [27–30], but for clarity, we outline here its main features with PMDA as the basic dianhydride (Fig. 1).

In the first step, the $Si_8O_{12}[(CH_2)_3NH_3^+Cl^-]_8$ (ammonium chloride salt)-functionalized POSS is dissolved at a concentration of 0.9 wt% in an aqueous solution with 0.1 mol L^{-1} sodium hydroxyde. Most ammonium groups are then converted to primary amines because of the alkaline pH. In parallel, a PMDA dianhydride solution of concentration 0.075 wt% is prepared in toluene (Fig. 1a). In the second step, the contact of both solutions leads to the formation of a polyPOSS-(amic acid) network via polycondensation at the water/toluene interface (Fig. 1b). The polyPOSS-(amic acid) is a free-standing film, but it can also be obtained as

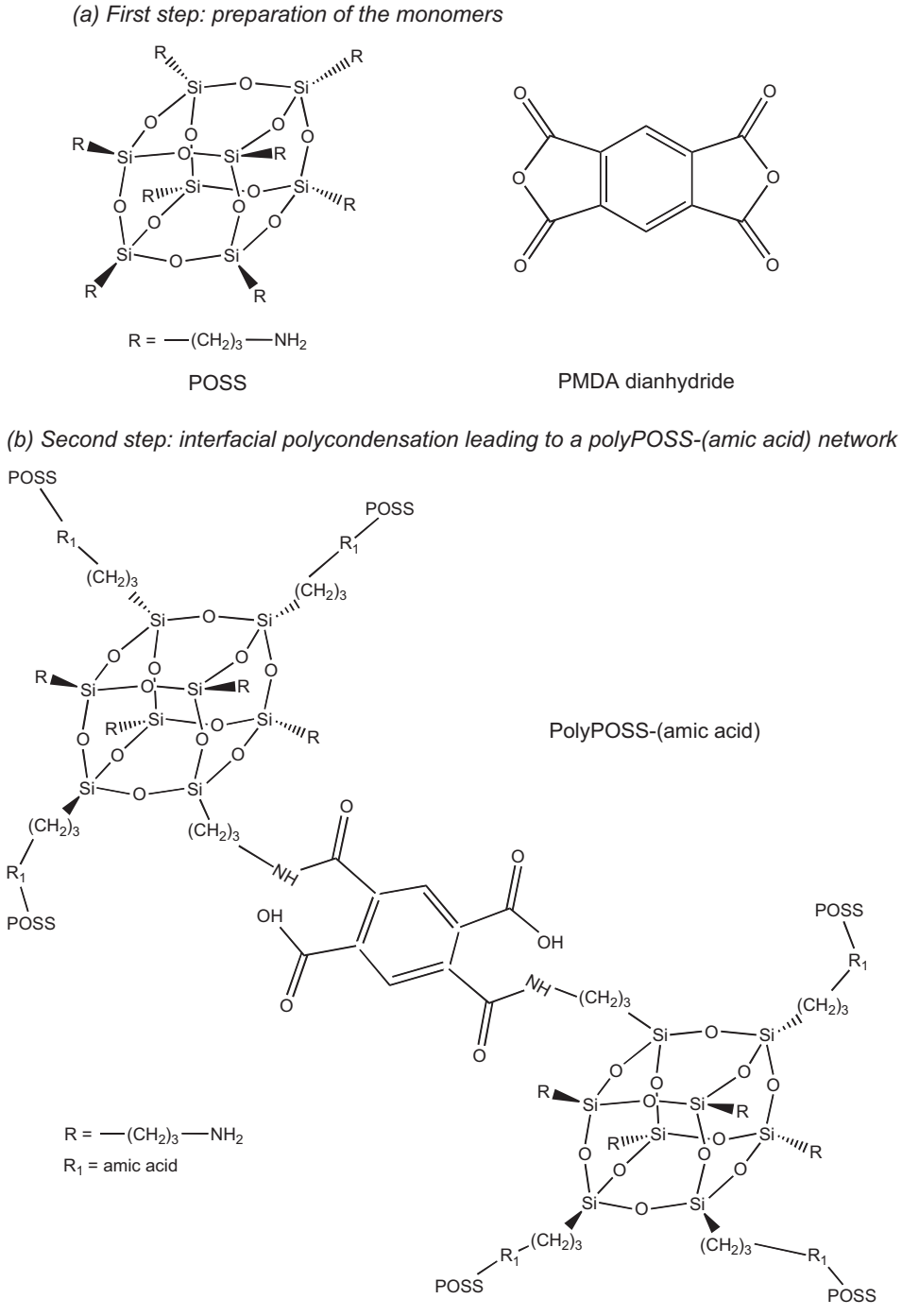

Fig. 1. Schematic representation of the synthesis of hyper-cross-linked polyPOSS-imide networks.

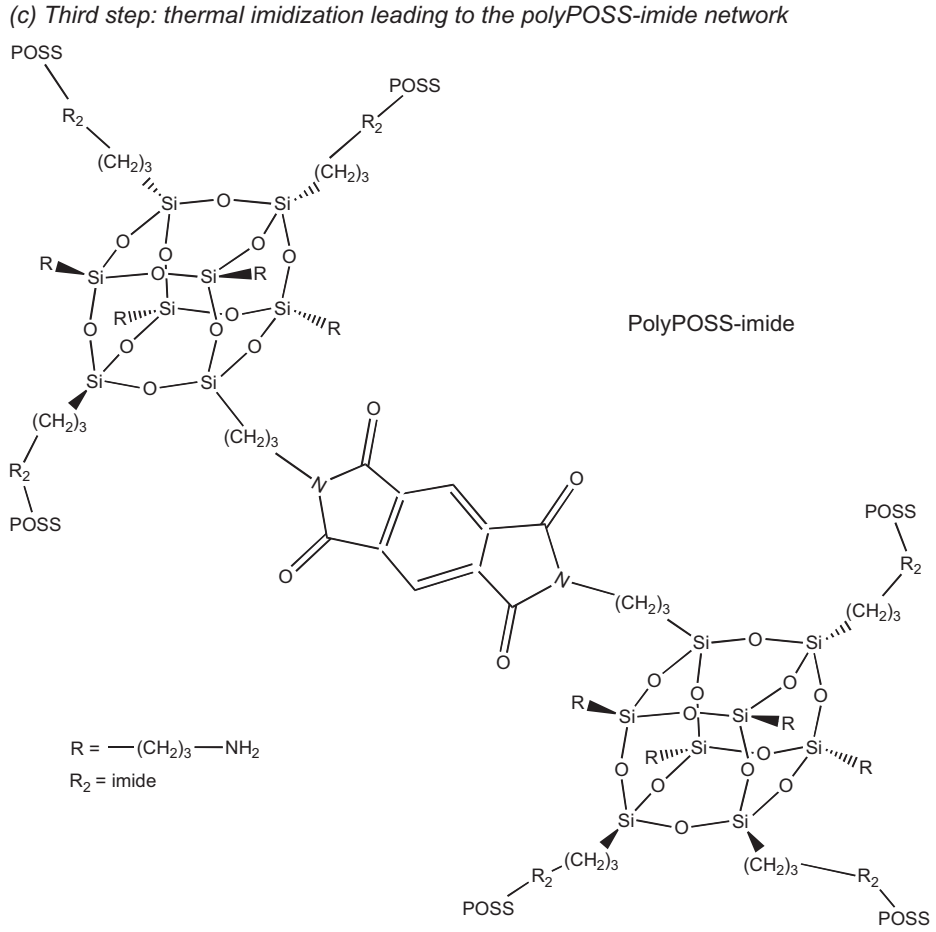

Fig. 1 (*continued*)

a supported film if a porous supporting structure is prewetted in the alkaline aqueous POSS solution before being contacted with the dianhydride solution in toluene. The third step involves the polyPOSS-(amic acid) being subsequently converted to a polyPOSS-imide film (Fig. 1c) by thermal treatment for 2 h at 300 °C under an atmosphere of air and at a heating rate of 5 °C min^{-1}. Over the entire process, residual reactants are washed off from the sample surfaces and the solvents are evaporated under dry nitrogen atmosphere.

The molecular modelling reaction scheme was designed to closely mimick the experimental conditions, but a few points had to be simplified. The POSS and PMDA monomers were created as bulk models rather than as solutions, since it would have been impossible in terms of current computational resources to create solutions at such high dilutions with both realistic solvents and enough monomers to give reasonable statistics in the networks. This could be further rationalized by the fact that the polycondensation reaction is necessarily governed by the high reactivity of the primary amines on POSS and the anhydride groups on PMDA. Indeed, due to the slow diffusion of the large POSS cages, the polycondensation reaction is completely confined to the liquid–liquid interface. This has been confirmed by *in-situ* visualizations of interfacial POSS/trimesoyl chloride polymerization layers [56], and is in contrast to regular interfacial polymerization reactions that proceed in the organic solvent. As such, the solvents play a less important role for these POSS-based networks. For the starting POSS model, it was deemed unnecessary to model the ammonium chloride-salt functionalization since the alkaline pH immediately converts the majority of ammoniums into amine groups before the polycondensation step. The POSS monomer models were thus all based on octa(aminopropylsilsesquioxane) $Si_8O_{12}[(CH_2)_3NH_2]_8$. Similarly, the porous supporting structure was not explicitly modelled, as the pores are typically of the order of several nanometers and do not influence the gas permeabilities, i.e. all model films were free-standing. A last simplification was related to the experimental infrared and XPS spectra suggesting that some POSS cages are partially hydrolyzed during the process [27,28,30]. This could be due to silanol groups being formed via a partial hydrolysis of POSS cages in the presence of NaOH in the aqueous solution used for interfacial polymerization, but it is probably somewhat counteracted by the fact that the opposite silanol condensation reactions occur during the heat treatment procedure [29,30]. Since the details of cage degradation are very difficult to assess unambiguously [57] (e.g. where it is degraded, which groups are hydrolyzed, if several parts of the same cage are degraded, if there are other side-reactions, etc.), it was decided instead to maintain the integrity of the POSS cages in the models.

3. Simulation details

All MD simulations were carried out using the *gmq* package [58], either in its scalar or in its parallel form, with a time step of $\Delta t = 10^{-15}$ s in the integration algorithm. In the force-field, the "bonded" interactions resulting from near-neighbor connections in the structures were described with angle-bending, torsional and out-of-plane potentials. To avoid problems of equipartition of kinetic energy, high-frequency modes, such as bond stretching

or fast motions of the hydrogens in explicit CH_2 and aromatic CH groups, were removed using rigid constraints with a relative tolerance of 10^{-6} [59]. The "nonbonded" excluded-volume van der Waals and electrostatic potentials, which depend on the distance between two interacting sites, were applied to all atom pairs situated either on the same molecule (but separated by more than two bonds if the intervening angles are subject to the bending potential or by more than one bond otherwise) or on two different molecules. All force-field parameters are given along with the atom-types in Appendix A (Fig. S1 and Table S1).

The long-range electrostatic potential was calculated using the Ewald summation method [60,61], and the three parameters controlling its convergence were systematically optimized [62]. Depending on the number of processors used, the real space cutoff R_c was typically set to 10–12 Å, the maximum integer defining the range of the reciprocal space sum K_{max} to 12–16 and the separation parameter α to 0.19–0.24. It should be noted that the partial charges (Fig. S1 in Appendix A) of the initial mixture, polyPOSS-(amic acid) and polyPOSS-imide forms were different, thus implicitely taking into account the fact that the charge distribution changes when chemical reactions occur [39]. The van der Waals cutoff was set to R_c and long-range corrections to the energy and the pressure were implemented [63]. Loose-coupling procedures [64,65] were used to maintain the temperature T and the pressure tensor $\boldsymbol{P}$ close to the required values with relaxation times of 0.1 ps for T and 5 ps for $\boldsymbol{P}$. Some initial simulations were run under constant-volume *NVT* conditions (constant number of atoms N, controlled volume V, controlled temperature T). The mixtures runs were performed under *NpT* conditions, in which the isotropic pressure p is controlled but the box is kept cubic and is allowed to relax toward its equilibrium size. Most other production runs were carried out under *NPT* conditions, in which the box size and shape are allowed to vary in response to the difference between the measured pressure tensor and the applied pressure tensor, i.e. on-diagonal components of the required pressure tensor are set to 1 bar and off-diagonal components are set to zero. Thermodynamic data were stored every 1 ps, configurational data every 5 ps for post-analyses, and systems were visualized using the VMD 1.8.7 software [66].

Several mechanical tests were also carried out. In the isotropic dilation tests, the required pressure was first reduced linearly at a rate of $dp/dt = -1$ bar/ps over 1000 ps, then maintained at ~−999 bar for 1000 ps before being linearly increased at a rate of +1 bar/ps back to 1 bar over 1000 ps and relaxed at this pressure for 1000 ps. In addition, uniaxial extension tests were made by changing the tension in the y direction at a rate of 1 bar/ps for 5000 ps at 22 °C and 4000 ps at 300 °C. The rate dependence of the mechanical properties was assessed by running an uniaxial extension test for one sample with a rate an order of magnitude slower (0.1 bar/ps), and by carrying out a creep test: the applied tension was fixed at the value obtained after 5000 ps at 1 bar/ps and the relaxation of the deformation was monitored for an extended time of 20,000 ps.

4. Preparation of the molecular networks

4.1. The POSS and PMDA monomer mixtures

To model the first step (Fig. 1a), bulk POSS and PMDA models were prepared separately. They were then mixed to prepare the starting configurations for the polycondensation reaction.

For the bulk POSS, three large boxes containing 216 POSS molecules were prepared using the same procedure as described in detail earlier [57]. Although preliminary tests were carried out with much smaller systems containing 32 POSS molecules, it was soon found that, with only a limited number of PMDA to choose from, the actual distributions of the number of links *per* POSS came out as being very noisy. In addition, small systems where connections can be made from one POSS molecule to its own image via the periodic boundaries (because of the temporary possibility of long links) should be avoided. As such, larger systems were used to get better statistics. With 216 POSS molecules at the start, our final boxes sizes of ~30,000 atoms for the networks were typically of the order of the largest systems used for epoxy-based simulations [41,43,44]. The production runs were performed up to 5000 ps at the experimental temperature of 22 °C. In parallel, PMDA bulk models of various sizes were prepared by carrying out *NVT* gas-phase simulations to randomize the molecules. The systems were then densified and relaxed with MD for 2000 ps at 22 °C. Experimentally, the average number of imide links per POSS has been shown to be four [27,28,30], which amounts to a stoechiometric ratio of two dianhydrides per POSS (2:1). Based on the hypothesis of volume additivity for the POSS + PMDA mixtures (the average molecular volumes being ~1240 Å^3 for a POSS and ~215 Å^3 for a PMDA molecule), the center-of-mass of each POSS molecule was subjected to affine scaling, thus slightly "separating" the POSS moieties. The scaled POSS boxes were then superimposed with dense PMDA boxes of the same sizes to test whether it was possible to select at least 432 PMDA molecules whose atoms were not overlapping with the atoms in the 216 POSS within a range of 3 Å. This condition also avoids the unphysical spearings and interlockings which can occur when superimposing ring- and cage-containing systems [67]. It was found that this meant having at least a ratio of 16 PMDA per POSS in terms of volumes, i.e. scaling the three POSS bulk boxes to lengths of ~100 Å, and consequently having to prepare three dense large PMDA boxes of a similar size. Table 1 displays the average equilibrium densities ρ_{model} and box lengths L of the pure bulk models, obtained over three systems each. In this work, averages are systematically presented with their associated standard error. Table 1 also reports the average molecular volumes and dimensions of the monomers. For POSS, the latter can be defined as twice the average distance between the center of a siloxane cage and its eight primary amine N, while for PMDA, it is the average distance between both anhydride O at the ends.

To our knowledge, the experimental density of solid $Si_8O_{12}[(CH_2)_3NH_2]_8$ has not been reported, but the density of the (ammonium chloride salt)-functionalized POSS was found by helium pycnometry to be ~1.35 g cm^{-3}. Considering the added molecular weight of the chloride ions and the hydrophilic nature of the salt, the model POSS density seems very reasonable. This is also the case for the disordered PMDA model, whose density falls rather close to the experimental crystal value of 1.68 g cm^{-3} [68]. In terms of molecular dimensions, the POSS molecules are on average twice as long as the PMDA dianhydrides.

The POSS + PMDA monomer mixtures were obtained using the following procedure:

(a) Prepare separately ~100 Å side length boxes of center-of-mass affine-scaled 216-molecule POSS and dense PMDA (Table 1).

Table 1
The bulk monomer models at 22 °C.

	POSS	PMDA
No. of molecules	216	4630
No. of atoms	25,056	83,340
ρ_{model}/g cm^{-3} (±0.001)	1.177	1.712
L/Å (±0.02)	64.53	99.30
Molecular volume/Å^3	1239 ± 1	216 ± 1
Molecular dimension/Å	14.14 ± 0.02	6.731 ± 0.001

(b) Superimpose both boxes and then select the requested number of PMDA (432/648/864 to get PMDA:POSS ratios of 2:1, 3:1, 4:1 respectively) that overlap the least with the POSS within a 3 Å range.
(c) Perform a 50,000 step energy minimization to remove the remaining overlaps.
(d) Switch to MD under *NpT* conditions at 227 °C to allow the mixture to come to equilibrium in the melt phase.
(e) Cool to 22 °C at a rate of −0.1 °C ps^{-1} and relax for an additional 2000 ps.

Although the experimental PMDA:POSS ratio is 2:1, there was concern that it would probably be difficult to link all the monomers if starting directly with a 2:1 model mixture. As such, mixtures with PMDA:POSS ratios of 3:1 and 4:1 were also prepared and tested for network formation. We emphasize that all resulting polyPOSS-(amic acid) and polyPOSS-imide networks will contain the experimentally-determined 2:1 ratio of PMDA to POSS. This is irrespective of whether they are obtained from a 2:1, 3:1 or 4:1 mixture, as in the latter two cases, all the excess unreacted PMDA will be removed after the formation of the network. The schematic representation of a relaxed 3:1 mixture in Fig. 2 shows that both types of monomers are well distributed in the dense mixtures. The characteristics of the various model mixtures are summarized in Table 2, and the model volumes V were found to be consistent with the ideal mixing volumes V_{ideal}, as obtained from the data for the pure PMDA and pure POSS systems given in Table 1. The density of the mixtures increases with increasing PMDA content as pure PMDA is much denser than pure POSS (Table 1). The un-cross-linked 2:1 mixture was further run under *NpT* conditions at 300 °C for 2000 ps to compare its characteristics to those of the cross-linked networks, which have the same PMDA:POSS ratio.

Table 2
The PMDA:POSS relaxed mixtures at 22 °C.

	2:1 ratio	3:1 ratio	4:1 ratio
No of molecules	648	864	1080
No of atoms	32,832	36,720	40,608
ρ_{model}/g cm^{-3} (±0.001)	1.310	1.358	1.395
L/Å (±0.1)	71.2	74.0	76.7
V/Å^3 (±50)	360,730	405,520	450,895
V_{ideal}/Å^3	360,150	405,790	451,430
V/V_{ideal}	1.002	0.999	0.999

4.2. The polycondensation

To model the polycondensation leading to the polyPOSS-(amic acid) (Fig. 1b), the PMDA:POSS mixtures had to be transformed into networks. Since experimental evidence suggests that none of the anhydride groups remain unreacted [27,28,30], the first assumption was that all dianhydrides must be connected to the arms of the POSS molecules at both ends. The schematic reaction mechanism, which is displayed in Fig. 3, implies then that each end of a PMDA dianhydride interacts with a primary amine on a POSS arm. Some of the atom-types used in the force-field (see Appendix A) change upon transformation of the monomers to the polyPOSS-(amic acid) network, as their chemical nature is modified.

During the condensation, a covalent bond is formed between the POSS nitrogen and one of the two ketone carbons on the PMDA anhydride. This leads to the opening of the ring through the breaking of the bond between the "attacked" ketone carbon and the ether oxygen. The reaction is completed by the transfer of a hydrogen from the amine N to the former ether oxygen to form a hydroxyl group. To simplify the procedure, it is assumed that both ends of the dianhydride molecule react at the same time to an amine N on different POSS arms, regardless of whether these arms belong to the same POSS cage or different ones. Both links can also be attached either in a *para* or in a *meta* conformation with respect to the central PMDA ring. While the formation of intramolecular bridges can be precluded in a cross-linking algorithm as implemented e.g. for epoxy-POSS nanocomposites [36], we do not make such restrictions here. The proportion of intermolecular ("interPOSS") to intramolecular bridges ("intraPOSS") as well as the proportion of *meta* to *para* links will thus be results of the transformation procedure.

The algorithm for building the polyPOSS-(amic acid) network from the relaxed mixtures was:

(a) For each PMDA dianhydride, find the unreacted POSS nitrogens closest to each of its four ketone carbons Ck.
(b) Select the nitrogen having the shortest Ck···N distance to one of the ketone carbons for each end of a PMDA and define the sum of these two minimal distances as R_{min}.
(c) Assuming that the most favorable linking situation is the lowest R_{min}, identify the PMDA to be reacted. The rare cases where both ends of a PMDA molecule are close to the same amine N are discarded.

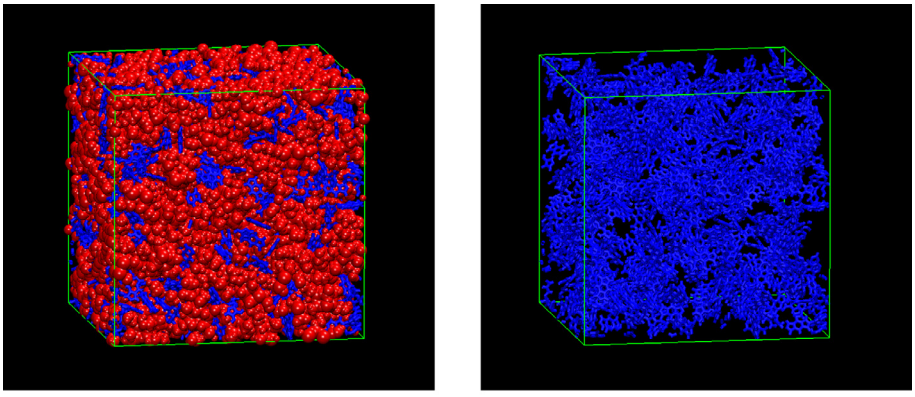

Fig. 2. A schematic representation of a 3:1 PMDA:POSS relaxed mixture (36,720 atoms) at 22 °C. The POSS are shown as space-filling red models, while the PMDA are represented with blue bonds: (a) is the entire mixture and (b) displays the distribution of the PMDA monomers within the mixture. (For interpretation of the references to color in this figure legend, the reader is referred to the web version of this article.)

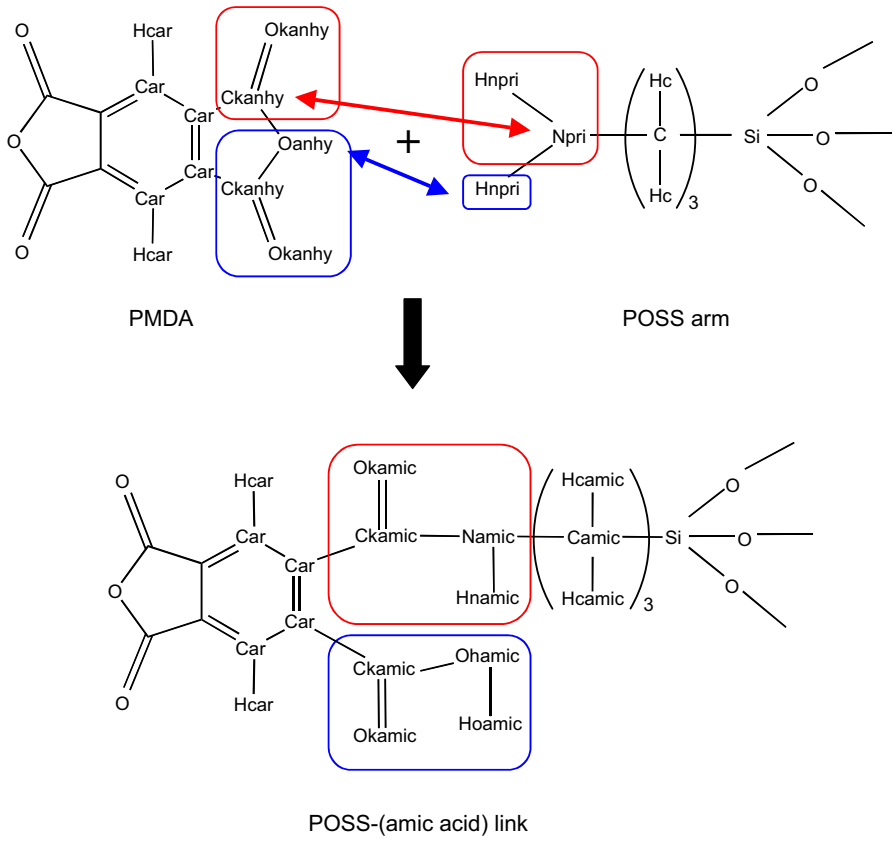

Fig. 3. The reaction of a PMDA dianhydride end with the amine group on a POSS arm to form a POSS-(amic acid) link. The atom-types are defined as in Appendix A.

(d) Perform the "reaction" at both ends by changing the connectivity, i.e. by breaking the anhydride C–O bond, forming the C–N bond and transfering the $-NH_2$ hydrogen that is closest to the former ether oxygen to the new hydroxyl oxygen (Fig. 3). Change the atom-types and charges, the latter of which depend on the type of link (*para* or *meta*) that is formed (see Appendix A).
(e) Return to (a) until the desired number of dianhydrides has reacted. At the end of the procedure, remove all unreacted PMDA molecules.

Radial distribution functions $g(r)$ show that the nearest distances between the POSS amine N and the PMDA ketone C are ~2.5 Å (Fig. S2 in Appendix A). The lowest value of R_{min} is thus expected to be ~5 Å. A comparison of the actual R_{min} obtained in PMDA:POSS mixtures of ratios 2:1, 3:1 and 4:1 (Fig. S3 in Appendix A) shows indeed that the dianhydrides can be ranked according to their proximity to the POSS and that the most favorable ones have R_{min} values of ~5 to 6 Å. The R_{min} increase fairly slowly with the rank for all ratios but in the 2:1 mixture, there is an upturn in the curve for the PMDA ranked higher than ~300 as it becomes increasingly difficult to find unreacted amine N close to the few remaining unreacted dianhydrides.

Two different approaches were tested to apply the transformation algorithm.

4.2.1. Instantaneous approach

In the instantaneous approach, all the reactions were made at the same time from a single mixture input configuration. As noted before, this led to some very long initial "bonds" (up to ~10 Å) being formed in the 2:1 mixture and even in the 3:1 and 4:1 mixtures, some of the newly formed C–N and O–H bonds were highly stretched. The distance r_{ij} between the bonded atoms i and j in these stretched bonds thus had to be reduced. This was carried out using energy minimization for 10,000 steps with the described force field, except that a harmonic flexible bond potential was used for the new C–N and O–H bonds (Eq. (1)):

$$\Phi_b(|\boldsymbol{r_{ij}}|) = \frac{1}{2}k_b(|\boldsymbol{r_{ij}}| - b_0)^2 \quad (1)$$

with k_b being the force constant and b_0 the equilibrium bond length. It was found by trial and error that k_b = 100 kg s^{-2} was sufficient to contract the C–N and O–H bond lengths back to their equilibrium values. Following a short constant-energy MD simulation to check that no remaining stretched bonds or high-energy interactions such as spearing were present and to allow a gradual thermalisation of the system, the new bonds could be rigidified.

4.2.2. Progressive approach

The second approach was a more progressive procedure, i.e. only the most favorable molecules at one instant were reacted and the system was first relaxed before attempting to create more links. This allowed some of the strain created by the formation of the links to be relaxed away between the reaction steps. The optimized procedure consisted in reacting only those PMDA where $R_{min} \leqslant 6$ Å in the first place, which effectively limited the length of the initially stretched C–N bonds to no more than ~3 Å. Following a reaction step, the system was energy-minimized for 1000 steps using the same harmonic potential for the C–N and O–H bonds as in the instantaneous approach (Eq. (1)), run for 1 ps under constant-energy conditions and then re-thermalized for 8 ps with *NVT* MD. After this cycle, another reaction step was attempted with the same criterion of $R_{min} \leqslant 6$ Å followed by the relaxation steps. If no reactions were possible, then a further 1 ps of *NVT* MD was car-

ried out before scanning the system again for possible reactions. This process continued over several hundred picoseconds until the required 432 PMDA had reacted with the 216 POSS; the exact simulation times for each sample generated using the progressive approach are given in Table 3. The excess PMDA molecules were subsequently removed. This progressive approach worked quite well for the 3:1 and 4:1 mixtures, but in the case of the 2:1 mixture, the reaction rate slowed down too much and could not go to completion in any reasonable time scale. To investigate the possible influence of the starting configuration of the PMDA + POSS mixtures, three independent samples were tested for the 3:1 ratio.

Table 3 summarizes the connectivity of the polyPOSS-(amic acid) systems generated using both the instantaneous and progressive methods, with the numbers and percentages for the intraPOSS links (links between two arms attached to the same POSS), the *para* and *meta* links as well as the number of atoms in the resulting network that are linked together and the time required to complete all the reactions. Fig. 4 gives the probability density distributions for the number of links per POSS molecule.

Both Table 3 and Fig. 4 show that, for all cases, the cross-linking process results in the formation of a network structure, in which practically all the original POSS molecules are joined together. Occasionally a POSS molecule ends up with zero links or it can be linked to a single PMDA, which somewhat isolates it from the rest of the network. However, these cases are relatively rare and more than 98% of the atoms are connected in the network structure. The isolated molecules are considered trapped within the network structure and are thus retained for the subsequent MD simulations.

Based on experimental evidence [27,28,30], all the model polyPOSS-(amic acid) systems were constructed with an average of 4 linked arms per POSS. However, the actual underlying distributions (Fig. 4) are quite wide with the range going from 0 links to the maximum possible, i.e. 8 links per POSS. These networks are thus highly heterogeneous. The frequency of *para* and *meta* links is systematically close to the expected 50/50 ratio, and ~10% to 20% of links are intraPOSS. The proportion of intraPOSS links is somewhat dependent on the PMDA:POSS ratio, as when the POSS are more "diluted", there are more chances of creating such links. IntraPOSS links are consistent with chain···chain interactions in POSS being fairly independent of whether the arms belong to the same siloxane cage or not [13], but it could also be partly due to the shortness of the PMDA moiety. Indeed, one could expect that steric hindrance does not favor such reactions for larger linkers. Various other characterizations including the energies, which are reported in Table S2 of Appendix A, did not reveal any obvious evidence of residual strains remaining in the systems obtained using the instantaneous approach. As such, even though the progressive approach initially appeared as the most reasonable, there was in fact no fundamental problems in using either the instantaneous or progressive approach.

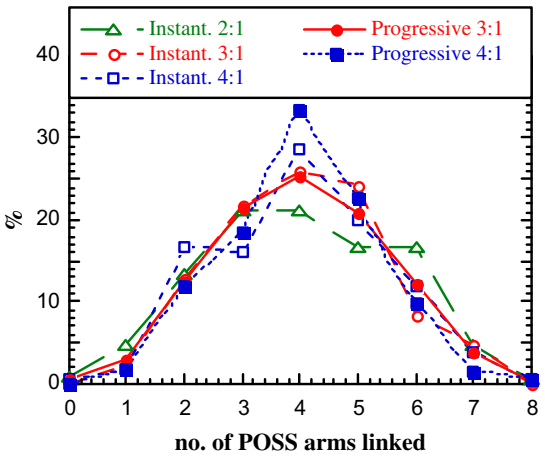

Fig. 4. Probability density distributions of the number of arms linked per POSS cage in the polyPOSS-(amic acid) networks generated either with the instantaneous or progressive approaches and starting with various PMDA:POSS mixtures. In the case of the progressive approach for the 3:1 mixture, the results have been averaged over three independent samples.

After the initial construction phase, the polyPOSS-(amic acid) networks were briefly relaxed under *NVT* conditions and then switched to *NPT* conditions. Since the density relaxation was very slow at 22 °C, the systems were heated and run at 300 °C for 10,000 ps to obtain a reasonable stabilization of the density, energies and conformational properties. This long annealing step was particularly critical for the conformational relaxation of the carboxylic groups. Indeed, it has been suggested that the rotation of the carboxylic group toward the amide group could be the rate-limiting step during the subsequent imidization [69] and that, when the rotational freedom is hindered by the POSS cage, it requires a larger activation energy than for conventional polyimides [29,30]. The relaxation function for the *trans* state of the (Ckamic)-Car-Car-Ckamic-Ohamic angle was calculated [70] at 300 °C and fitted to a stretched exponential KWW (Kohlrausch–Williams–Watts) form [71]. The area under this curve gave a correlation time of 6800 ± 20 ps. However, in the cases where the amide N–H does not point in the direction of the carboxylic group, the amide N–H has to rotate towards the carboxylic group to be able to form an imide bond. From the initial decay of the relaxation function for the *trans* state of the corresponding (Ckamic)-Car-Car-Ckamic-Namic angle, one could estimate this correlation time as being at least 250 times longer. As such, it is probably more of a rate-limiting step than the rotation of the carboxylic group.

Table 3
The connectivity of polyPOSS-(amic acid) networks prepared with different procedures.[a]

Reaction method	Instantaneous			Progressive (reactions if $R_{min} \leqslant 6$ Å)				
PMDA:POSS ratio in original mixture	2:1	3:1	4:1	3:1				4:1
				Sample 1	Sample 2	Sample 3	Average	
No. of intraPOSS links	45 (~10%)	71 (~16%)	92 (~21%)	63 (~15%)	84 (~19%)	66 (~15%)	*71 (~16%)*	91 (~21%)
No. of *para* links	214 (~50%)	233 (~54%)	222 (~51%)	233 (~54%)	205 (~47%)	208 (~48%)	*~215 (~50%)*	216 (50%)
No. of *meta* links	218 (~50%)	199 (~46%)	210 (~49%)	199 (~46%)	227 (~53%)	224 (~52%)	*~217 (~50%)*	216 (50%)
No. of atoms in continuous network (out of 32,832)	32,332 (~98.5%)	32,394 (~98.7%)	32,296 (~98.4%)	32,314 (~98.4%)	32,314 (~98.4%)	32,698 (~99.6%)	*32,442 (~98.8%)*	32,278 (~98.3%)
Time required to complete all reactions/ps	–	–	–	632	1211	711	*851*	340

[a] For the 3:1 mixture using the progressive approach, values are given for each of the three independent samples as well as the corresponding averages.

After their 10,000 ps relaxation at 300 °C, the polyPOSS-(amic acid) systems were subsequently cooled back to 22 °C at a rate of −0.1 °C ps^{-1} and simulated for a further 4000 ps. The final configurations were used both for the subsequent imidization and for the mechanical tests. Since the instantaneous and progressive approaches appeared to work equally well, all results were systematically averaged over the seven systems of Table 3 to improve the statistics. A schematic representation of a polyPOSS-(amic acid) network is provided in Fig. 5.

4.3. The thermal imidization

To model the thermal imidization leading to the polyPOSS-imides (Fig. 1c), the polyPOSS(amic acid) networks have to undergo a condensation reaction of the amide group and the adjacent carboxylic acid with the production of water as a side product. Experimentally, this step is carried out up to 300 °C, water is readily removed from the system as it evaporates at such temperatures and the reaction is complete after 2 h [27–30]. The schematic reaction mechanism which is given in Fig. 6, leads to the POSS cages being connected via diimide bridges.

The algorithm for converting the polyPOSS-(amic acid) into polyPOSS-imide networks was:

(a) For each amide group, create a bond between the nitrogen atom and the carbonyl carbon in the adjacent carboxylic acid group.
(b) Eliminate the hydroxyl group (Ohamic and Hoamic) and the amide nitrogen (Hnamic) as a water molecule.
(c) Change the atom-types and charges (see Appendix A).

Since the connectivity is directly defined by the polyPOSS-(amic acid) networks, all the transformations could be performed simultaneously. However, because of the different possible conformations of the amide and carboxylic acid groups, some of the initial C–N bonds were stretched out to ~4 Å. As before, these long links were relaxed using energy minimization and the flexible bond potential of Eq. (1), although a larger k_b of 500 kg s^{-2} was required to ensure the rotation of those (Ckamic)-Car-Car-Ckamic-Namic angles that were not initially into the required *cis* state. A short constant-energy MD was performed before rigidifying the new bonds. The polyPOSS-imide networks were then run under *NVT* conditions at 300 °C for 100 ps before continuing the simulations under *NPT* conditions up to 5000 ps. The systems were cooled back to 22 °C at −0.1 °C ps^{-1} and then further relaxed up to 9000 ps. As for the polyPOSS-(amic acid)s, the differences in energies between the polyPOSS-imides and the un-cross-linked 2:1 mixture, which are reported in Table S3 of Appendix A, show that they are very similar for all seven systems under study. However, the polyPOSS-imide networks have a less negative potential energy than the polyPOSS-(amic acid) intermediates, which, as will be shown later, is related to the rigidity of the imide fragment and their lower density. A schematic representation of a polyPOSS-imide network is provided in Fig. 7.

5. Characterization of the molecular networks

The bulk, structural and mechanical properties of the intermediate and final model systems, i.e. the 2:1 PMDA:POSS unlinked mixture, the polyPOSS-(amic acid) and the polyPOSS-imide networks, were characterized and confronted whenever possible to available experimental evidence [27–30]. To have good statistics, analyses for the polyPOSS-(amic acid)s were systematically averaged over the seven 32,832-atom systems of Table 3, and those for the polyPOSS-imides over the corresponding seven 30,240-atom systems.

5.1. Bulk properties

Table 4 presents the average model densities ρ_{model} and box lengths/thicknesses $L = V^{1/3}$ at 22 °C and 300 °C, along with the volumetric thermal expansion coefficient α_V which can be expressed both in terms of volume V or density ρ:

$$\alpha_V = \frac{1}{V}\left(\frac{\partial V}{\partial T}\right)_P = -\frac{1}{\rho}\left(\frac{\partial \rho}{\partial T}\right)_P \quad (2)$$

and the linear thermal expansion coefficient α_L, which is obtained for an isotropic system from α_V by:

$$\alpha_L = \frac{\alpha_V}{3} \quad (3)$$

Since the density-temperature cooling plots were fairly linear for the networks, the slopes were estimated from the differences between the ρ_{model} obtained at 22 °C and 300 °C. For the unlinked mixture, the cooling curve was less linear, so the slope was estimated in the range 22–77 °C.

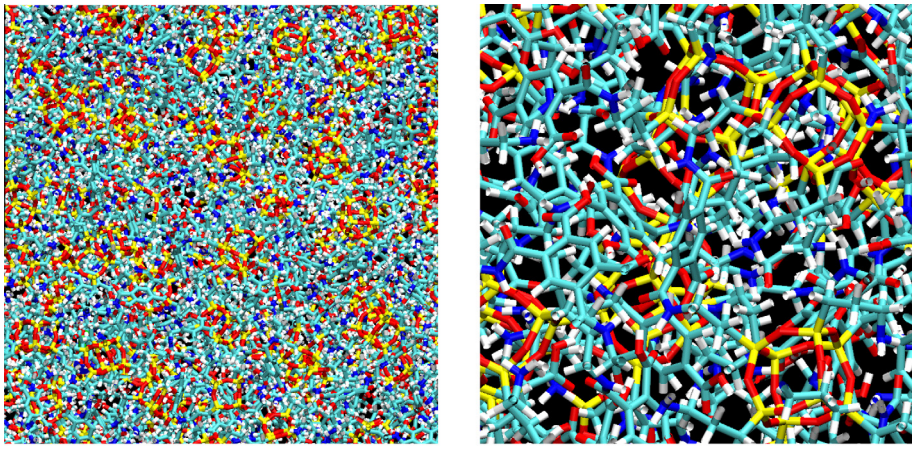

Fig. 5. Schematic representation of a polyPOSS-(amic-acid) network at 22 °C. It originates from a 3:1 mixture transformed using the progressive approach: (a) is the entire 32,832-atom system and (b) is a close-up representation of (a). The color code is the following: yellow = Si, red = O, cyan = C, blue = N, white = H. (For interpretation of the references to color in this figure legend, the reader is referred to the web version of this article.)

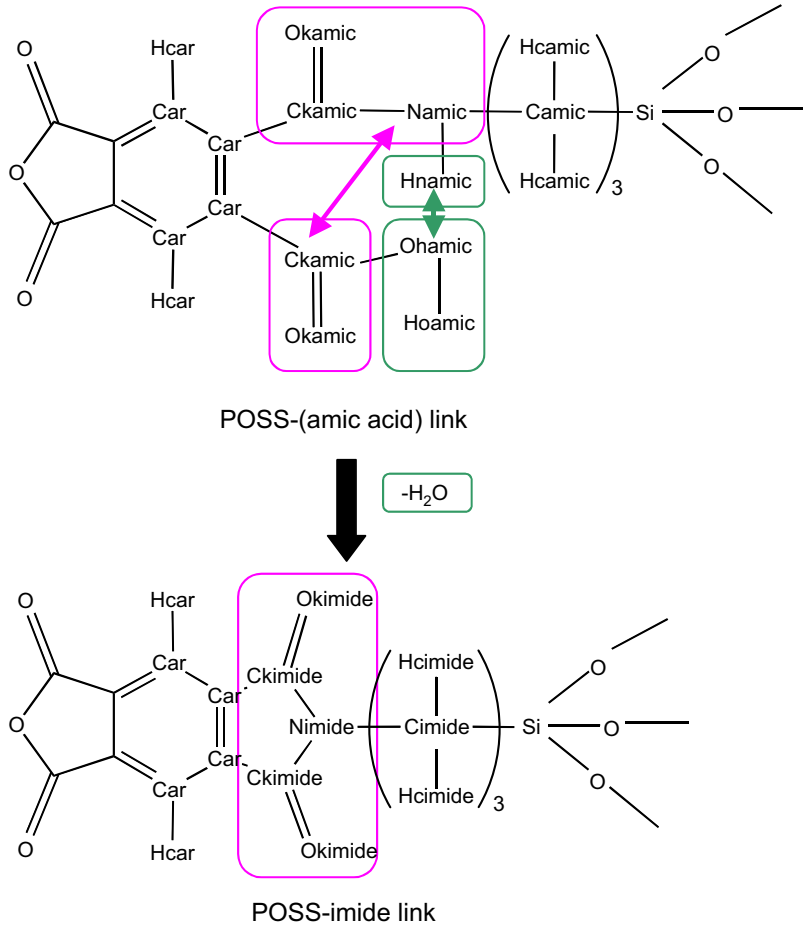

Fig. 6. The conversion of a POSS-(amic acid) into a POSS-imide link. The atom-types are defined as in Appendix A.

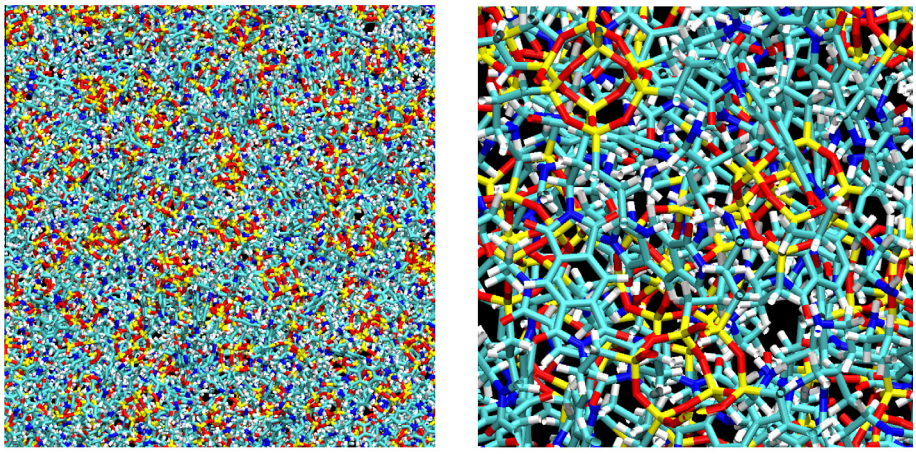

Fig. 7. Schematic representation of a polyPOSS-imide network at 22 °C. It originates from the system shown in Fig. 5 and the color code is the same: (a) is the entire 30,240-atom system and (b) is a close-up representation of (a). (For interpretation of the references to color in this figure legend, the reader is referred to the web version of this article.)

As expected, the formation of a network decreases the density and thermal expansion coefficients as the linked systems are sterically more constrained and more difficult to deform when the temperature is raised. In addition, the films experience further thickness and density reduction during the imidization process due to the removal of water. The experimentally-measured linear thermal expansion coefficient for the polyPOSS-imides based on PMDA is 76×10^{-6} °C^{-1} [29,30], and is thus in excellent agreement with our model α_L value of $(74 \pm 2) \times 10^{-6}$ °C^{-1} (Table 4). Following imidization, the average thickness shrinks by $1.1 \pm 0.1\%$ at 22 °C, which is also coherent with the decrease in refractive index observed by thermo-ellipsometry [29,30]. In the models, this

Table 4
The model densities and thicknesses at both 22 °C and 300 °C.

	2:1 PMDA:POSS mixture	polyPOSS-(amic acid)	polyPOSS-imide
ρ_{model} at 22 °C/g cm^{-3} (±0.002)	1.310	1.253	1.221
ρ_{model} at 300 °C/g cm^{-3} (±0.002)	1.128	1.175	1.145
$\alpha_V/10^{-6}$ °C^{-1} (±5)	280	225	223
L at 22 °C/Å (±0.1)	71.2	72.3	71.5
L at 300 °C/Å (±0.1)	74.8	73.8	73.1
$\alpha_L/10^{-6}$ °C^{-1} (±2)	93	75	74

corresponds to a volume shrinkage of ~3% and a mass decrease of ~5.5%, which explains the slight reduction in the density. However, the direct comparison with experiment is not particularly straightforward. Indeed, even if the changes during imidization are reduced with respect to un-cross-linked PMDA-ODA polyimides [72], a lot of the water present in the experimental hybrid networks is not directly linked to the reaction step. Thermogravimetry indicates that polyPOSS-(amic acid) powders undergo a mass loss of ~10% between 50 °C and 300 °C, while ellipsometry suggests a difference of ~25% in film thicknesses at 50 °C before and after imidization. The large majority of this additional water has been associated to physically bound water, the loss of which during heating overlaps with the imidization step, along with water released during side-reactions involving the silanol condensation of partially hydrolyzed cages [29,30]. On the other hand, the models do not have any residual solvent and their cages are all intact. Their water loss is thus restricted to the actual imidization reaction.

5.2. Void spaces

There are many ways to characterize void-spaces in molecular simulations but the results usually depend on the definition of the void-space and the various approximations that have to be made [1,73]. Since the networks are intended for gas separation applications, it is preferable to characterize the void-space available to a specific type of probe molecule based on energetic rather than geometric criteria [74,75], e.g. with a test-particle insertion (TPI) method [76]. Here a N_2 gas molecule with the potential parameters of Vrabec et al. [77] was repeatedly inserted at random positions in the systems and the changes in potential energies $\Delta\Phi$ associated with the virtual insertions were recorded. N_2 was used as a probe as it does not lead to any conditioning effects. Information on the energies of likely sites for gas adsorption can be obtained from the Boltzmann-weighted probability density distributions for the changes in potential energy [78], which are displayed both at room (22 °C) and at high (300 °C) temperatures in Fig. 8a and b. The integral under these curves gives the solubility,

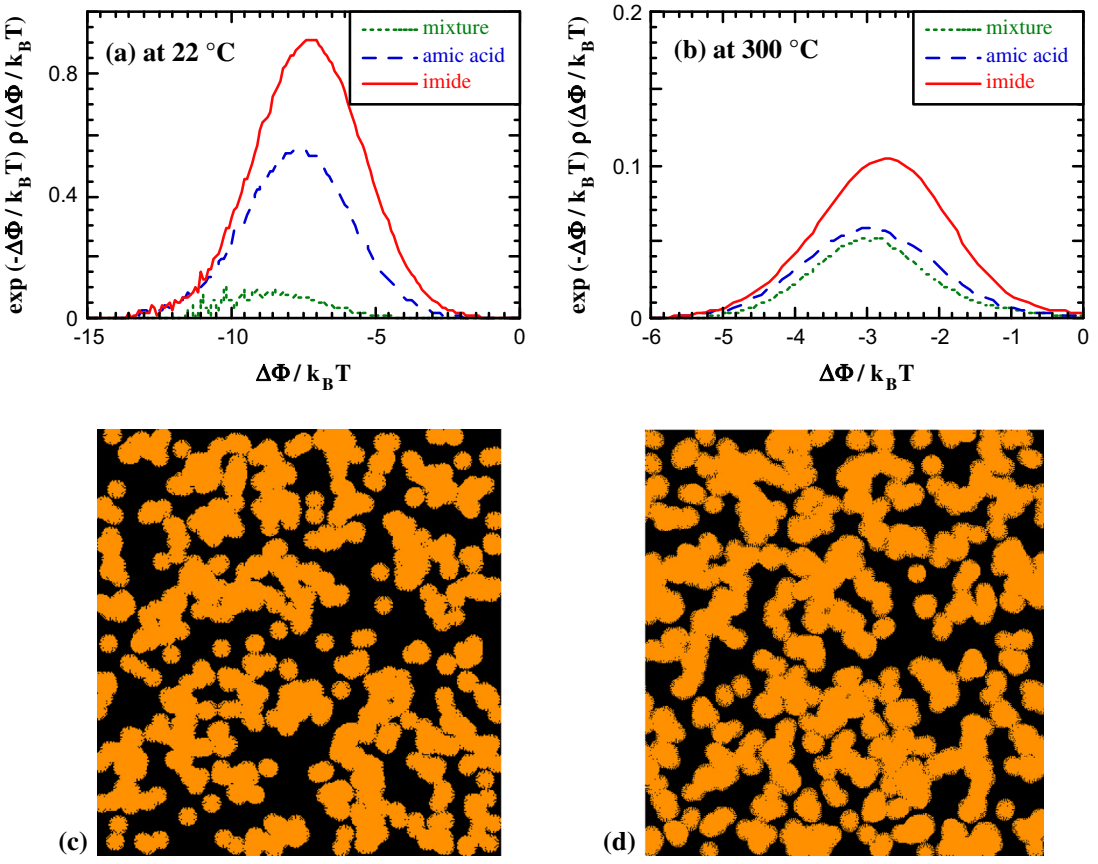

Fig. 8. Boltzmann-factor-weighted probability density distributions for the insertion energy of a N_2 gas probe in the 2:1 PMDA:POSS mixture, the polyPOSS-(amic acid) and polyPOSS-imide networks at (a) 22 °C and (b) 300 °C. k_B is Boltzmann's constant (c) and (d) are schematic representations of the 1000 most favorable sites for the insertion of N_2 into a polyPOSS-imide network at 22 °C and 300 °C, respectively.

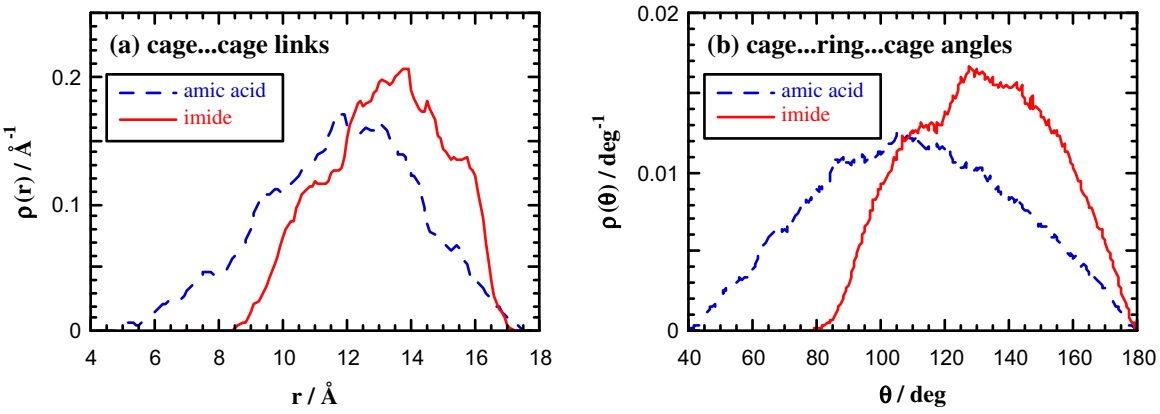

Fig. 9. Normalized probability density distributions before and after imidization for (a) the interPOSS cage···cage link distances and (b) the interPOSS cage···ring···cage pseudo-angles.

Table 5
The average values for significant link distances and angles in the networks at 22 °C.

	polyPOSS-(amic acid)	polyPOSS-imide
InterPOSS cage···cage links/Å	11.79 ± 0.08	13.23 ± 0.05
IntraPOSS cage···cage links/Å	3.28 ± 0.01	3.33 ± 0.01
InterPOSS cage···ring···cage angles/deg	110.7 ± 0.9	132.3 ± 0.4
IntraPOSS cage···ring···cage angles/deg	30.4 ± 0.1	35.4 ± 0.2

and lower insertion energies are associated to the most favorable sites [73].

The actual solubilities in units of $cm^3(STP)\,cm^{-3}\,cmHg^{-1}$ at room temperature were 0.004 ± 0.001 for the mixture, 0.031 ± 0.001 for the polyPOSS-(amic acid)s and 0.052 ± 0.001 for the polyPOSS-imides, which are consistent with those found for N_2 in conventional polyimides [79–81]. Using the fraction of random insertions in the systems leading to energies that contribute to 99.9% of the solubility, the fraction of significant volume available to the N_2 probe at 22 °C was estimated to 0.05% for the mixture, 0.62 ± 0.03% for the polyPOSS-(amic acid)s and 1.50 ± 0.03% for the polyPOSS-imides. The same analyses at 300 °C gave estimations of 1.34% for the mixture, 1.57 ± 0.04% for the polyPOSS-(amic acid)s and 2.94 ± 0.06% for the polyPOSS-imides. It is clear that the amount of significant void space, i.e. the space that is available to the N_2 probe, increases in the order unlinked mixture < polyPOSS-(amic acid)s < polyPOSS-imides. This agrees once again with the decrease in density upon cross-linking along with the minor shrinkage and the decrease in refractive index upon imidization for the PMDA-based networks [29,30], which confirms that both cross-linking and imidization create additional free volume because of the enhanced steric constraints. When the temperature increases, the concomitant decrease in density also creates additional free volume. However, as shown by comparing Fig. 8a and b, it should be pointed out that solubility is not only correlated to the available void-space: lower densities do lead to more space for the penetrants, i.e. higher solubility, but they also lead to a lower cohesive energy density, i.e. less solubility [82]. Solubility will thus be a compromise between available space and cohesive energy. The insertion energies are clearly less favorable at 300 °C than at 22 °C, and indeed the actual solubility for N_2 in units of $cm^3(STP)\,cm^{-3}\,cmHg^{-1}$ goes down to 0.0015 ± 0.0001 for the polyPOSS-imides. Although this should be somewhat compensated by a faster diffusion, it could contribute to the excellent permselectivity measured for H_2/N_2 in the polyPOSS-imide networks based on PMDA [28,30].

The most energetically favorable inserted probes ($\Delta\Phi/k_BT < -10$) in the polyPOSS-imides at both 22 °C and 300 °C are visualized [75] in Fig. 8c and d. At both low and high temperatures, the favorable sites for N_2 remain clearly well spread out within the network. As found before [13], these sites are always situated in the organic phase and form some connected channels which, in cooperation with the mobility of the network, will provide the paths at the basis of gas permeation.

5.3. Structural analyses

The structural differences between the polyPOSS-(amic acid) and polyPOSS-imide networks were characterized in terms of distances and angles. Fig. 9 compares the probability density distributions for the interPOSS (links attached to different cages) cage···cage distances and cage···ring···cage pseudo-angles. The "cage" positions were the linking silicons and the "ring" positions were set at the center of the organic aromatic rings. Table 5 gives the average values corresponding to Fig. 9 both for interPOSS and intraPOSS (links between two arms attached to the same cage) connections.

Fig. 9 confirms that these networks are very heterogeneous as the interPOSS angles span ranges of 140° for the polyPOSS(amic acid)s and 100° for the polyPOSS(imide)s. Imidization leads to a stiffening of the material with larger link distances and angles, which slightly pushes the POSS cages away from each other. However, in both cases, some links are almost linear while others can be very kinked. The angles are even smaller when the imide is linked to the same siloxane cage and the distances suggest that the linking Si are either near-neighbors or at least on the same siloxane face. The intraPOSS links, which amount to ~10% to 20% of the total number (Table 3) thus form constrained loops at the surface of the siloxane cages. As shown by Figs. S4 and S5 in Appendix A, the ends of the planar imide moiety in such intraPOSS links are slightly bent, the angles next to the imides are shifted towards smaller values and those next to the siloxane cages

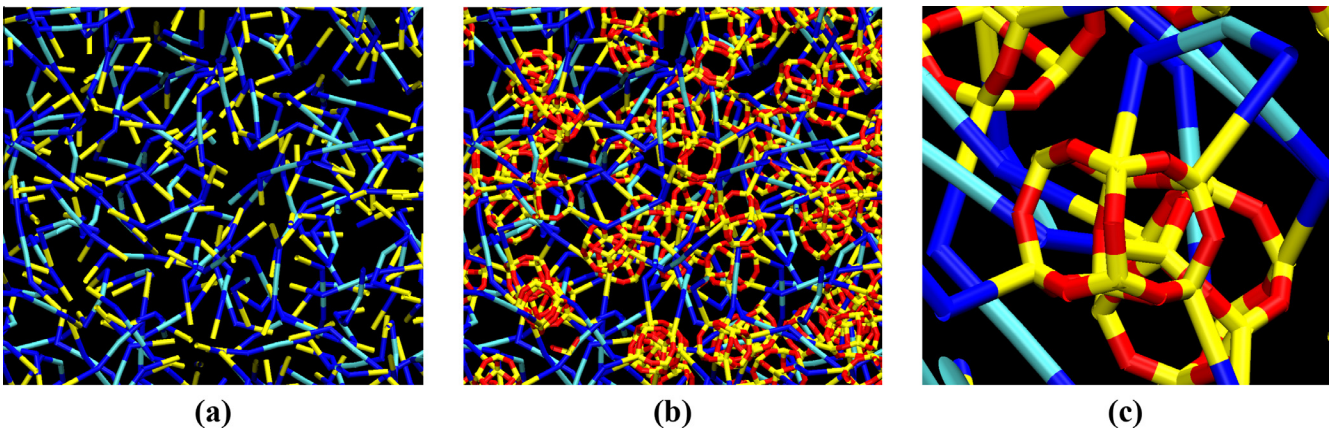

Fig. 10. Simplified representations of the organic links as pseudo cage···N···ring···N···cage bonds in a 30,240-atom polyPOSS-imide network at 22 °C. (a) Shows the organic links on their own, (b) the same as (a) but with the siloxane cages and (c) is a close-up representation of a siloxane cage forming both intraPOSS (top right corner) and interPOSS links. The color code is as in Figs. 5–7. (For interpretation of the references to color in this figure legend, the reader is referred to the web version of this article.)

towards larger values with respect to the interPOSS-link majority. Interestingly, these differences between intraPOSS and interPOSS links are almost non-existent in the polyPOSS-(amic acid) intermediate. This confirms that the flexibility of the amic acid arm allows for the creation of the link, irrespective of whether the POSS arms belong to the same cage or not. It is only over the imidization stage, i.e. after the actual formation of the network, that the transformation of the amic acid into the rigid imide moiety adds constraints to the intraPOSS links. Since it has been shown experimentally that the conversion from the amic acid to the imide form is complete [27–30], we have to assume that such intraPOSS links do occur as well in the real material in spite of the strain they induce. The heterogeneity of the connectivity and the differences between interPOSS and intraPOSS links are further illustrated in Fig. 10, which displays simplified representations of part of a polyPOSS-imide network, in which the organic links are shown as sequences of pseudo cage···N···ring···N···cage "bonds".

As suggested by Fig. 10, the imide moiety remains essentially planar and the cages do not deform significantly (see Fig. S4 for N···N and Fig. S6 for Si···Si distances in Appendix A). Such an extended range of cage···ring···cage angles can only be explained by the large flexibility of the $-(CH_2)_3-$ linker between the organic moieties and the siloxanes cages. Fig. 11 compares the probability density distributions for the successive torsional angles in the linkers before and after imidization. In the convention used here, a dihedral angle τ varies from $-180°$ to $+180°$, with $-60° < \tau < 60°$ being a *trans* conformation. Similarly, the *gauche* conformations are those angles situated either in the $-180° \leqslant \tau \leqslant -60°$ or in the $60° \leqslant \tau \leqslant 180°$ intervals. In the angle names, the first atom mentioned is the one closer to the siloxane cage.

As found before for amino-functionalized POSS [57], the key dihedral angles are those in the middle of the linker, i.e. Si–C–C–C and C–C–C–N. The O–Si–C–C and C–C–N–Ck angles have much lower barriers to rotation and as such, are less discriminative. Indeed, the polyPOSS-imides O–Si–C–C distribution (Fig. 11b) shows that the direct link to the siloxane cage can basically adopt any value. Both the Si–C–C–C and C–C–C–N angles are initially half in linear *trans* forms and half in coiled *gauche* forms in the polyPOSS-(amic acid) films. Upon imidization, the C–C–C–N *trans* contribution decreases significantly from ~50% to ~35%,while the Si–C–C–C angles are less affected. The increase of *gauche* conformations is also apparent in the C–C–N–Ck angles. This is partly due to the intraPOSS links, which are so strained that all their conformers for the Si–C–C–C and C–C–N–Ck angles become *gauche*. However, even in the case of the interPOSS links, imidization leads to more coiled structures for the flexible linker in order to better accommodate the stiff imide moiety.

5.4. Mechanical analyses

The mechanical properties of the unlinked and the cross-linked model systems were investigated at both 22 °C and 300 °C by ramping up and down the appropriate required pressure tensor ***P*** components and measuring the associated changes in densities

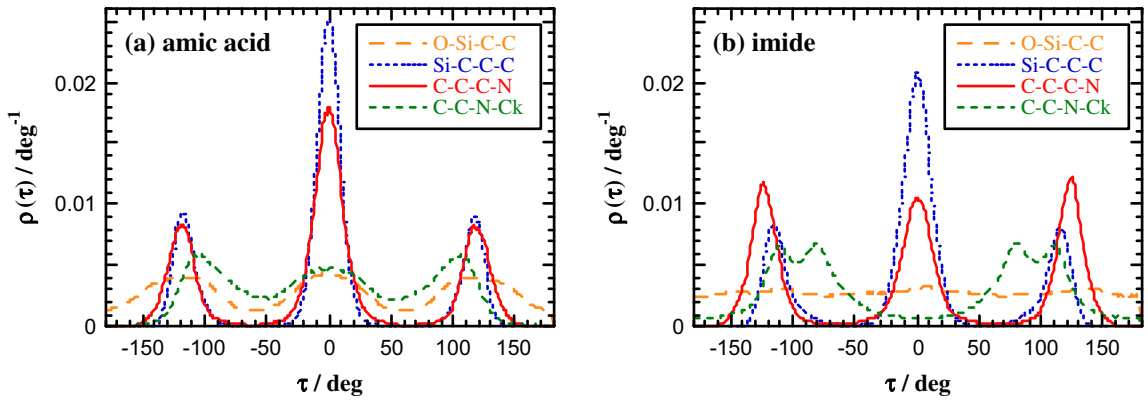

Fig. 11. Normalized probability density distributions for the torsional angles in the $-(CH_2)_3-$ linker between the inorganic and the organic moieties (a) before and (b) after imidization.

Table 6
The mechanical properties.

	2:1 PMDA:POSS mixture	polyPOSS-(amic acid)	polyPOSS-imide
Bulk modulus K at 22 °C/GPa	4.66 ± 0.04	4.9 ± 0.1	3.85 ± 0.08
Young's modulus E at 22 °C/GPa	5.6 ± 0.2	5.9 ± 0.2	5.1 ± 0.1
Poisson's ratio at 22 °C	0.38 ± 0.01	0.31 ± 0.03	0.30 ± 0.03
Young's modulus E at 300 °C/GPa	–	2.2 ± 0.4	2.4 ± 0.4
Poisson's ratio at 300 °C	–	0.31 ± 0.06	0.31 ± 0.06

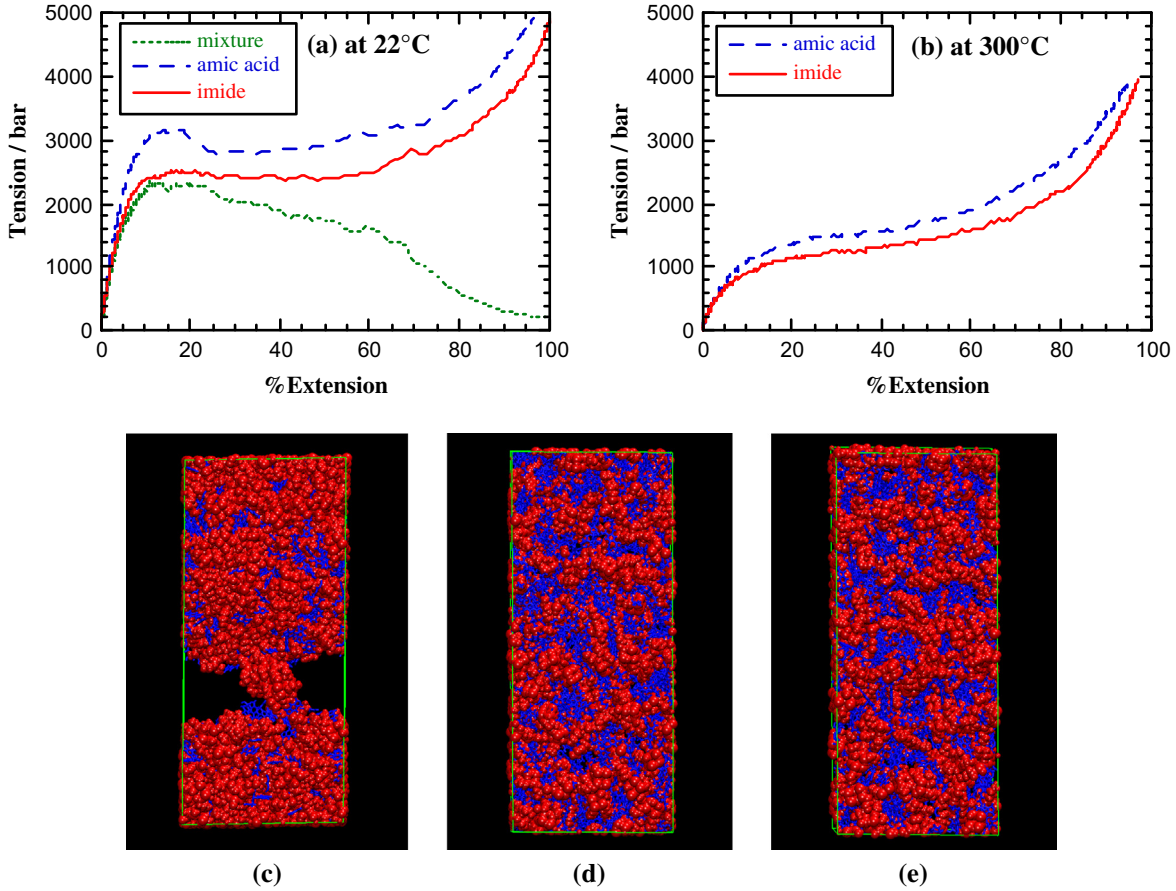

Fig. 12. Tensile stress–strain curves at (a) 22 °C and (b) 300 °C along with (c–e) schematic representations of systems at extensions of ~90% for the 2:1 PMDA:POSS mixture, a polyPOSS-(amic acid) and a polyPOSS-imide network, respectively. The inorganic POSS are shown as space-filling red models, while the organic moieties are represented with blue bonds. The respective number of atoms are 32,832 for the mixture and polyPOSS-(amic acid) and 30,240 for the polyPOSS-imide. (For interpretation of the references to color in this figure legend, the reader is referred to the web version of this article.)

and strains. Although, the model induced strain rates are necessarily much higher than in experiment because of the limited timescale available to MD simulations, the systems could be compared under similar conditions. The bulk moduli K were obtained from the slopes of the pressure–density curves. The tensile Young's moduli E were obtained from the slopes of the stress-strain curve at low deformations and Poisson's ratio from the transverse vs axial strains. Their averages are presented in Table 6, while the stress–strain curves at room and high temperatures are compared in Fig. 12a and b. Schematic representations of the various systems at 90% extension and at 22 °C are displayed in Fig. 12c–e.

The moduli at both 22 °C and 300 °C are consistent with reinforced glassy organic materials. Although we do not have available experimental data to compare directly with as the actual films are supported [27,29,30], the model results are of the same order of magnitude than moduli reported in simulations of epoxy-based networks, which have been found to be consistent with experimental data [37,39,42,43,50,83,84]. The networks do not behave as typical rubbers and this is confirmed by the Poisson's ratios that are representative of stiff materials [34,41,85].

At 22 °C and low deformations, the stress–strain curves (Fig. 12a) all exhibit a fairly similar behavior up to yield strains of ~10% to 20%. It has been reported that cross-linking reduces Young's modulus in POSS-polyurethanes [86]. This agrees with our unlinked mixture behaving at low deformations in a similar way to the networks, which indicates that the reinforcement effect is indeed more governed by the presence of the inorganic particles than by the covalent bonding. At larger deformations, the un-cross-linked mixture loses its cohesion and eventually starts to cavitate (Fig. 12c). On the other hand, the networks display a ductile behavior typical of cold-drawing before showing a clear strain hardening effect (Fig. 12a, e, and f), which is related to the orientation of the organic moieties in the direction of the tension (Fig. S7 in Appendix

A). As such, cross-linking prevents failures such as that shown in Fig. 12c from occurring.

At 300 °C, the mixture behaves as a liquid upon application of the uniaxial tension, i.e. the on-diagonal elements all decrease together (not shown) and the material flows. At low extensions, the networks deform more easily than at 22 °C with no apparent yield stresses, but strain hardening still occurs at high extensions (Fig. 12b). Their Poisson's ratios remain close to 0.3 and their Young's moduli E are ~2 GPa (Table 6), which confirms the resistance of these stiff materials at elevated temperatures.

In such MD simulations, the mechanical properties of polymer-based materials are known to be somewhat dependent on both the rate of deformation and the thermal history of the sample [84,87,88]. In order to assess the dependence on the deformation rate, an additional stress–strain simulation of a polyPOSS-imide network was carried out with a lower rate of 0.1 bar/ps instead of 1 bar/ps. The elastic modulus and yield stress were, as expected, slightly lower at the lower deformation rate. However, at large deformations, the network connections lead to an elastic behavior that is fairly independent of the deformation rate. This was confirmed by a creep test of the same polyPOSS-imide system at 22 °C carried out by fixing the applied tension at the value obtained after 5000 ps at 1 bar/ps (~90% deformation, Fig. 12a and e) and monitoring the deformation for an extended time of 30,000 ps. The deformation soon reached a plateau, thus confirming that there is not much scope for relaxation left in this cross-linked system, and as such, that the rate dependence at high deformations is minor. Both these simulations are presented in Appendix A (Fig. S8). As for the dependence on the cooling rate, the rates used here (0.1 °C ps^{-1}) are very slow for large MD simulations and, as noted above, the point here is to compare the relative mechanical properties simulated under similar conditions. However, simulations of epoxy networks have shown that if the cooling rate does affect the yield stress, samples with different thermal histories will collapse into a single curve once inelastic deformation begins [84].

If one compares the intermediate and the final networks, the polyPOSS-(amic acid)s systematically exhibit higher yield stresses and strain hardenings than the polyPOSS-imides. Following imidization, K at 22 °C is reduced by ~21% and E by ~14%, i.e. a lot more than the average density reduction of 2.6% (Table 4). It is probably the larger amount of free volume in the polyPOSS-imides which leads to the differences between the two curves. However, at 300 °C, this tends to be reduced despite the similar volumetric thermal expansion coefficients (Table 4) and indeed, both E are close within the errors (Table 6). There is less relative difference in the fractions of significant volume available to a gas probe and the added stiffness of the imide is probably an asset at such high temperatures.

6. Conclusions

This work successfully introduced methods for building realistic molecular models of hyper-cross-linked polyPOSS-imide films based on the PMDA dianhydride. Relaxed dense samples of the POSS and PMDA monomers were first prepared on their own, before being combined to form mixtures with PMDA:POSS ratios of 2:1, 3:1 and 4:1. Two different algorithms were presented to mimick the polycondensation step which transforms the POSS + PMDA mixtures into polyPOSS-(amic acid) networks by creating amide and carboxylic acid groups. This step was carried out using either an instantaneous approach, i.e. all the links were created at the same time, or a more progressive approach, which allowed for some relaxation in between the formation of the links. However, the various PMDA:POSS mixture ratios and transformation routes gave similar polyPOSS-(amic acid) networks, thus suggesting that all of these procedures worked equally well. In all cases, more than 98% of the atoms were connected in a continuous network, *para* and *meta*-connected links had an equal probability and ~80% to 90% links were interPOSS. Although the models were constructed with the experimentally-found average of 4 links per POSS, the actual distributions of the number of links *per* POSS were wide with all possible values ranging from zero to eight arms. The subsequent thermal imidization step leading to the final polyPOSS-imide films involved the condensation reaction of the amide and the adjacent carboxylic acid with the production of water as a side product. Since the connectivity was directly defined by the polyPOSS-(amic acid) precursors, all the transformations could be performed simultaneously.

Both the formation of a network and the imidization reaction decreased the density and increased the available void-space as the linked systems are sterically more constrained. The volume shrinkage during the imidization step was significantly less than expected from the amount of water removed. The model thermal expansion coefficient for the polyPOSS-imides was found to be in remarkable agreement with the experimental value. The decrease in model thickness upon imidization also agreed with experiment.

In terms of structures, the model networks were found to be highly heterogenous. The cage···ring···cage pseudo-angles covered an extended range of values, which was related to the large flexibility of the $-(CH_2)_3-$ linker between the organic moieties and the siloxanes cages. It even allowed the intraPOSS links to form loops at the surface of the siloxane cages. However, it is only over the imidization stage, i.e. after the actual formation of the network, that the transformation of the amic acid into the rigid imide moiety added constraints to the intraPOSS links. In general, imidization favored more coiled structures for the flexible linker to better accomodate the stiff planar imide moiety. It also had a tendency to push away the POSS cages, thus gaining additional free-volume.

At room temperature, all the systems under study exhibited good mechanical properties at low deformations. At larger deformations, the unlinked mixture eventually cavitated, while the networks experienced strain hardening instead. At higher temperature, the mixture was liquid and the networks were slightly easier to deform but they retained their capacity to strain hardening and their moduli remained quite large. The dependence of such mechanical properties on the deformation rate was limited. Cross-linking thus clearly improved the overall mechanical resistance.

Although gas permeation was not the main subject of the present work, these polyPOSS-imide networks were developed to maintain good gas separation performances at high temperatures and pressures [27–30]. As far as solubility is concerned, the model networks based on the PMDA moiety already show a good compromise between available space and cohesive energy, with the favorable sites for gas motion being situated in the organic phase. Model networks based on other imide moieties are under preparation and their comparative gas separation properties will be the subject of future work.

Acknowledgments

This work was performed within the frameworks of the Institute for Sustainable Process Technology (www.ispt.eu) and the Centre of Excellence of Multifunctional Architectured Materials "CEMAM" n° ANR-10-LABX-44-01. It was granted access to the HPC resources of CCRT/CINES/IDRIS under the allocations 2014- and 2015-095053 made by GENCI (Grand Equipement National de Calcul Intensif), France. The MUST cluster at the University Savoie Mont Blanc (France) is also acknowledged for the provision of computer time.

Appendix A. Supplementary material

Supplementary data associated with this article can be found, in the online version, at http://dx.doi.org/10.1016/j.commatsci.2016.02.015.

References

[1] Y. Yampolskii, Macromolecules 45 (2012) 3298.
[2] L.M. Robeson, J. Membr. Sci. 320 (2008) 390.
[3] L.M. Robeson, J. Membr. Sci. 62 (1991) 165.
[4] B.W. Rowe, L.M. Robeson, B.D. Freeman, D.R. Paul, J. Membr. Sci. 360 (2010) 58.
[5] L.M. Costello, W.J. Koros, J. Polym. Sci., Part B: Polym. Phys. 33 (1995) 135.
[6] S. Kim, S.H. Han, Y.M. Lee, J. Membr. Sci. 403–404 (2012) 169.
[7] M. Calle, C.M. Doherty, A.J. Hill, Y.M. Lee, Macromolecules 46 (2013) 8179.
[8] K. Vanherck, G. Koeckelberghs, I.F.J. Vankelecom, Prog. Polym. Sci. 38 (2013) 874.
[9] B.S.R. Reddy, Advances in Nanocomposites – Synthesis, Characterization and Industrial Applications, InTech, Rijeka, Croatia, 2011.
[10] T. Moore, W.J. Koros, J. Mol. Struct. 739 (2005) 87.
[11] F. Peng, L. Lu, H. Sun, Y. Wang, J. Liu, Z. Jiang, Chem. Mater. 17 (2005) 6790.
[12] D.B. Cordes, P.D. Lickiss, F. Rataboul, Chem. Rev. 110 (2010) 2081.
[13] S. Neyertz, P. Gopalan, P. Brachet, A. Kristiansen, F. Männle, D. Brown, Soft Mater. 12 (2014) 113.
[14] F. Männle, T. Tofteberg, M. Skaugen, H. Bu, T. Peters, P.D.C. Dietzel, M. Pilz, J. Nanopart. Res. 13 (2011) 4691.
[15] H. Rios-Dominguez, F.A. Ruiz-Trevino, R. Contreras-Reyes, A. Gonzalez-Montiel, J. Membr. Sci. 271 (2006) 94.
[16] N. Hao, M. Böhning, A. Schönhals, Macromolecules 43 (2010) 9417.
[17] W.R. Kang, A.S. Lee, S. Park, S.-H. Park, K.-Y. Baek, K.B. Lee, S.-H. Lee, J.-H. Lee, S. S. Hwang, J.S. Lee, J. Membr. Sci. 475 (2015) 384.
[18] M.M. Raman, V. Filiz, M.M. Khan, B.N. Gacal, V. Abetz, React. Funct. Polym. 86 (2015) 125.
[19] F. Li, T.-S. Chung, S. Kawi, J. Membr. Sci. 356 (2010) 14.
[20] P. Iyer, G. Iyer, M. Coleman, J. Membr. Sci. 358 (2010) 26.
[21] B. Dasgupta, S.K. Sen, S. Banerjee, Mater. Sci. Eng. B 168 (2010) 30.
[22] D. Gnanasekaran, P.A. Walter, A.A. Parveen, B.S.R. Reddy, Sep. Purif. Technol. 111 (2013) 108.
[23] D.M. Pinson, G.R. Yandek, T.S. Haddad, E.M. Horstman, J.M. Mabry, Macromolecules 46 (2013) 7363.
[24] H. Pan, Y. Zhang, H. Pu, Z. Chang, J. Power Sources 263 (2014) 195.
[25] C. Gong, Y. Liang, Z. Qi, H. Li, Z. Wu, Z. Zhang, S. Zhang, X. Zhang, Y. Li, J. Membr. Sci. 476 (2015) 364.
[26] X.-F. Lei, M.-T. Qiao, L.-D. Tian, P. Yao, Y. Ma, H.-P. Zhang, Q.-Y. Zhang, Corros. Sci. 90 (2015) 223.
[27] M.J.T. Raaijmakers, M.A. Hempenius, P.M. Schön, G.J. Vancso, A. Nijmeijer, M. Wessling, N.E. Benes, J. Am. Chem. Soc. 136 (2014) 330.
[28] M.J.T. Raaijmakers, M. Wessling, A. Nijmeijer, N.E. Benes, Chem. Mater. 26 (2014) 3660.
[29] M.J.T. Raaijmakers, E.J. Kappert, A. Nijmeijer, N.E. Benes, Macromolecules 48 (2015) 3031.
[30] M.J.T. Raaijmakers, Doctoral thesis, University of Twente, The Netherlands, 2015.
[31] M. Dalwani, J. Zheng, M. Hempenius, M.J.T. Raaijmakers, C.M. Doherty, A.J. Hill, M. Wessling, N.E. Benes, J. Mater. Chem. 22 (2012) 14835.
[32] M. Ding, A. Szymczyk, F. Goujon, A. Soldera, A. Ghoufi, J. Membr. Sci. 458 (2014) 236.
[33] I. Yarovsky, E. Evans, Polymer 43 (2002) 963.
[34] C. Wu, W. Xu, Polymer 47 (2006) 6004.
[35] V. Varshney, S.S. Patnaik, A.K. Roy, B.L. Farmer, Macromolecules 41 (2008) 6837.
[36] P.-H. Lin, R. Khare, Macromolecules 42 (2009) 4319.
[37] T.C. Clancy, S.J.V. Frankland, J.A. Hinkley, T.S. Gates, Polymer (2009) 2736.
[38] P.-H. Lin, R. Khare, J. Therm. Anal. Calorim. 102 (2010) 461.
[39] C. Li, A. Strachan, Polymer 51 (2010) 6058.
[40] H. Hörstermann, R. Hentschke, M. Amkreutz, M. Hoffmann, M. Wirts-Rütters, J. Phys. Chem. B 114 (2010) 17013.
[41] N.B. Shenogina, M. Tsige, S.S. Patnaik, S.M. Mukhopadhyay, Macromolecules 45 (2012) 5307.
[42] N. Nouri, S. Ziaei-Rad, Macromolecules 44 (2011) 5481.
[43] A. Bandyopadhyay, P.K. Valavala, T.C. Clancy, K.E. Wise, G.M. Odegard, Polymer 52 (2011) 2445.
[44] A. Bandyopadhyay, G.M. Odegard, Model. Simul. Mater. Sci. Eng. 20 (2012) 045018.
[45] D.R. Heine, G.S. Grest, C.D. Lorenz, M. Tsige, M.J. Stevens, Macromolecules 37 (2004) 3857.
[46] L.J. Abbott, C.M. Colina, Macromolecules 44 (2011) 4511.
[47] J.H. Moon, A.R. Katha, S. Pandian, S.M. Kolake, S. Han, J. Membr. Sci. 461 (2014) 89.
[48] X. Song, Y. Sun, X. Wu, F. Zeng, Comput. Mater. Sci. 50 (2011) 3282.
[49] P.V. Komarov, C. Yu-Tsung, C. Shih-Ming, P.G. Khalatur, P. Reineker, Macromolecules 40 (2007) 8104.
[50] H. Liu, M. Li, Z.-Y. Lu, Z.-G. Zhang, C.-C. Sun, T. Cui, Macromolecules 44 (2011) 8650.
[51] A.A. Gavrilov, P.V. Komarov, P.G. Khalatur, Macromolecules 48 (2015) 206.
[52] S. Queyroy, S. Neyertz, D. Brown, F. Müller-Plathe, Macromolecules 37 (2004) 7338.
[53] M.K. Glagolev, A.A. Lazutin, V.V. Vasilevskaya, Macromol. Symp. 348 (2015) 14.
[54] N. Lacevic, R.H. Gee, A. Saab, R. Maxwell, J. Chem. Phys. 129 (2008) 124903.
[55] J.M. Ilnytskyi, M. Saphiannikova, D. Neher, M.P. Allen, Soft Matter 8 (2012) 11123.
[56] Y. Zhang, N.E. Benes, R.G.H. Lammertink, Lab Chip 15 (2015) 575.
[57] S. Neyertz, D. Brown, M. Pilz, N. Rival, B. Arstad, F. Männle, C. Simon, J. Phys. Chem. B 119 (2015) 6433.
[58] D. Brown, The gmq User Manual Version 5: available at <http://www.lmops.univ-savoie.fr/brown/gmq.html>, 2013.
[59] K.D. Hammonds, J.-P. Ryckaert, Comput. Phys. Commun. 62 (1991) 336.
[60] P.P. Ewald, Ann. Phys. 369 (1921) 253.
[61] W. Smith, Comput. Phys. Commun. 67 (1992) 392.
[62] D. Fincham, Mol. Simul. 13 (1994) 1.
[63] M.P. Allen, D.J. Tildesley, Computer Simulation of Liquids, Clarendon Press, Oxford, UK, 1987.
[64] H.J.C. Berendsen, J.P.M. Postma, W.F. Van Gunsteren, A. Dinola, J.R. Haak, J. Chem. Phys. 81 (1984) 3684.
[65] D. Brown, J.H.R. Clarke, Comput. Phys. Commun. 62 (1991) 360.
[66] W. Humphrey, A. Dalke, K. Schulten, J. Mol. Graph. 14 (1996) 33.
[67] S. Neyertz, Soft Mater. 4 (2007) 15.
[68] S. Aravamudhan, U. Haeberlen, H. Irngartinger, C. Krieger, Mol. Phys. 38 (1979) 241.
[69] M.K. Ghosh, K.L. Mittal, Polyimides: Fundamentals and Applications, Marcel Dekker Inc., New York, 1996.
[70] D. Brown, J.H.R. Clarke, J. Chem. Phys. 92 (1990) 3062.
[71] F. Müller-Plathe, J. Chem. Phys. 108 (1998) 8252.
[72] E. Unsal, M. Cakmak, Macromolecules 46 (2013) 8616.
[73] S. Neyertz, in: E.M.V. Hoek, V.V. Tarabara (Eds.), Encyclopedia of Membrane Science and Technology, John Wiley & Sons, Hoboken, NJ, 2013.
[74] S. Neyertz, D. Brown, Macromolecules 46 (2013) 2433.
[75] S. Neyertz, D. Brown, J. Membr. Sci. 460 (2014) 213.
[76] B. Widom, J. Chem. Phys. 39 (1963) 2808.
[77] J. Vrabec, J. Stoll, H. Hasse, J. Phys. Chem. B 105 (2001) 12126.
[78] S. Pandiyan, D. Brown, S. Neyertz, N.F.A. Van Der Vegt, Macromolecules 43 (2010) 2605.
[79] M.R. Coleman, W.J. Koros, J. Polym. Sci., Part B: Polym. Phys. 32 (1994) 1915.
[80] C.K. Yeom, J.M. Lee, Y.T. Hong, K.Y. Choi, S.C. Kim, J. Membr. Sci. 166 (2000) 71.
[81] L. Wang, Y. Cao, M. Zhou, X. Ding, Q. Liu, Q. Yuan, Polym. Bull. 60 (2008) 137.
[82] N.F.A. Van Der Vegt, W.J. Briels, M. Wessling, H. Strathmann, J. Chem. Phys. 105 (1996) 8849.
[83] H.B. Fan, M.M.F. Yuen, Polymer 48 (2007) 2174.
[84] C. Li, A. Strachan, Polymer 52 (2011) 2920.
[85] G.N. Greaves, A.L. Greer, R.S. Lakes, T. Rouxel, Nat. Mater. 10 (2011) 823.
[86] K.N. Raftopoulos, S. Koutsoumpis, M. Jancia, J.P. Lewicki, K. Kyriakos, H.E. Mason, S.J. Harley, E. Hebda, C.M. Papadakis, K. Pielichowski, P. Pissis, Macromolecules 48 (2015) 1429.
[87] A.V. Lyulin, M.A.J. Michels, Phys. Rev. Lett. 99 (2007) 085504.
[88] S.V. Lyulin, S.V. Larin, A.A. Gurtovenko, V.M. Nazarychev, S.G. Falkovich, V.E. Yudin, V.M. Svetlichnyi, I.V. Gofman, A.V. Lyulin, Soft Matter 10 (2014) 1224.